Ultra-Trace PFAS Detection Using Amplifying Fluorescent Polymers

Alberto Concellón‡, Jesús Castro-Esteban, and Timothy M. Swager*

Department of Chemistry, Massachusetts Institute of Technology, 77 Massachusetts Avenue, Cambridge, Massachusetts 02139, United States.

ABSTRACT: Per- and polyfluoroalkyl substances (PFAS) are environmentally persistent pollutants that are of growing concern due to their detrimental effects at ultra-trace concentrations (ng/L) in human and environmental health. Suitable technologies for on-site ultra-trace detection of PFAS do not exist and current methods require complex and specialized equipment, making the monitoring of PFAS in distributed water infrastructures extremely challenging. Herein, we describe amplifying fluorescent polymers (AFPs) that can selectively detect perfluorooctanoic acid (PFOA) and perfluorooctane sulfonate (PFOS) at concentrations of ng·L^{-1}. The AFPs are highly fluorinated and have poly(*p*-phenylene ethynylene) and polyfluorene backbones bearing pyridine-based selectors that react with acidic PFAS via a proton-transfer reaction. The fluorinated regions within the polymers partition PFAS into polymers, whereas the protonated pyridine units create lower-energy traps for the excitons, and emission from these pyridinium sites results in red-shifting of the fluorescence spectra. The AFPs are evaluated in thin film and nanoparticle forms, and can selectively detect PFAS concentrations of ~1 ppb and ~100 ppt, respectively. Both polymer films and nanoparticles are not affected by the type of water, and similar responses to PFAS were found in milliQ water, DI water, and well water. These results demonstrate a promising sensing approach for on-site detection of aqueous PFAS in the ng/L range.

INTRODUCTION

Per- and polyfluoroalkyl substances (PFAS) are "forever chemicals" and their high chemical stability allow them to slowly accumulate over time in the environment as well as in living systems.[1-3] Fluorinated materials have useful properties and are widely employed in consumer products including food packaging, nonstick cookware, lubricants, additives in fire-fighting foams, cleaning and personal care products. Their wide-spread use had aroused concern as a result of studies conducted by the Center of Disease Control and Prevention (CDC) which revealed that most people in the United States have been exposed to PFAS concentrations that may lead to detrimental health outcomes, such as thyroid disease, liver damage, reduced fertility, and even certain types of cancer.[4-8] There are multiple types of PFAS, however "long-chain" perfluoroalkyl carboxylic acids ($C_nF_{2n+1}COOH$, n≥7) and perfluoroalkyl sulfonic acids ($C_nF_{2n+1}SO_3H$, n≥6) show particularly resistance to degradation and are more bioaccumulative than their "short-chain" analogues.[9] In response, the US Environmental Protection Agency (EPA) released a health advisory level of 70 ng·L^{-1} (70 ppt) for a combined concentration of perfluorooctanoic acid (PFOA) and perfluorooctane sulfonate (PFOS) in drinking water.[10] This health advisory limit, that was issued in 2016, was revised in June 2022, and the current drinking water health advisories are 0.02 ppt for PFOA and 0.004 ppt for PFOS.[11] On March 2023, the US EPA announced a proposed National Primary Drinking Water Regulation for six different PFAS, with legally enforceable levels of 4 ppt for PFOA and PFOS as individual contaminants.[12] Such updated advisory levels are cautionary that some negative effects may occur with PFOA and PFOS concentrations in water that are at ultra-trace levels that are challenging to measure throughout distributed water infrastructures.

Current US EPA methods for the detection of PFAS at the ng/L range rely on combinations of liquid chromatography and mass spectroscopy.[13,14] Although these methods provide accuracy and sensibility, they are cost-prohibitive requiring specialized laboratories with well-trained personnel. Recent research efforts have been focused on developing fast, portable, user-friendly, low-cost detection methods that will allow for continuous environmental monitoring.[9, 15-25] However, few sensors are suitable for on-site detection, and they further lack sufficient sensitivity and/or selectivity. In addition to the ultra-low concentrations of PFAS in water, the complexity of real water samples, which usually contain various ions, biopolymers, humic acids, organic oils or surfactants, make PFAS detection, monitoring and mitigation extremely challenging.

Herein we show how the self-amplifying properties of fluorescent conjugated polymers enable the detection of aqueous PFAS at ng·L^{-1}. Signal amplification in amplifying fluorescent polymer (AFP) systems is the result of highly efficient excited state (exciton) transport along the polymer backbones and between neighboring polymers.[26-29] The rapidly diffusing excitons in some cases can sample thousands of polymer repeating units increasing the probability of encountering an analyte of interest (PFAS in the present case). If the presence of the analyte either causes a lower energy trapping state or a quenching site, the exciton is captured. AFPs are advantageous when compared to alternative fluorescent sensors since they exhibit larger signal amplification, exceptional sensitivity (i.e., femtogram detection limits), and in some cases, allow for naked-eye detection. Another key feature of AFPs is that sensing devices can be readily prepared by depositing AFP coatings onto glass, fiber optics or waveguides, or by dispersing AFPs in water to produce colloidal particles. Indeed, our group demonstrated the utility of AFPs in a diverse array of chemical and biological sensing applications, and in some cases these methods have proved to be robust enough to be implemented in commercial sensing devices.[30-34]

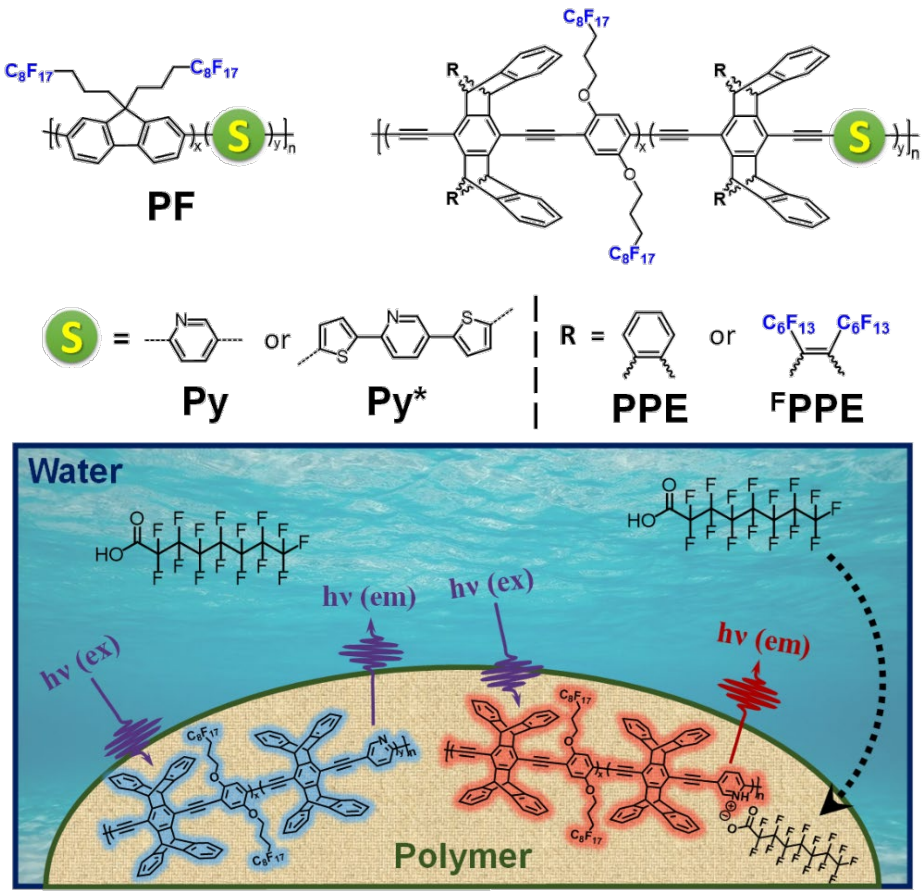

Figure 1. Chemical structure of the fluorous conjugated polymers (x= 0.80, y= 0.20) and conceptual scheme of the mechanism for the detection of PFAS in water: PFOA diffusion from water to the polymer induces protonation of the pyridine moieties and triggers changes in the emission of the polymers.

We report here a new sensing platform based on fluorescent polymers that specifically bind and respond to PFAS in aqueous environments. Our method relies on highly fluorinated polymers with poly(*p*-phenylene ethynylene) (PPE) and polyfluorene (PF) backbones bearing pyridine-based selectors that react with acidic PFAS (i.e., PFOA and PFOS) via a proton-transfer reaction (**Figure 1**). The fluorinated domains within the polymer backbone partition PFAS into polymers,[35-37] while the protonated pyridine units produce new emissive signals that are amplified by excitonic energy transport. Specifically, we designed two acidic PFAS selectors (**Py** and **Py*** in **Figure 1**), where the π-electron delocalizing character of the thiophene bridges in **Py*** triggers larger changes in fluorescence after protonation, in comparison to the simple pyridine selector (**Py**). As for the polymer backbones, we selected three different polymers (**PF**, **PPE** and **^{F}PPE** in **Figure 1**), which impede aggregation, allowing for spectroscopic stability and high emission efficiency in thin film and particle forms. In the case of **PPE** and **^{F}PPE** polymers, the rigid pentiptycene repeating units introduce molecular-level porosity that facilitates PFAS diffusion into solid polymers.[33] Moreover, both **PF** and **^{F}PPE** polymers possess a particularly high fluorine content (see **Table 1**) that increases PFAS affinity for the polymers.

Table 1. Molecular weight and polydispersity indices of the synthesized polymers.

	wt. % F[a]	M_n (g/mol)[b]	M_w (g/mol)[b]	$Đ_M$[b]
PF-Py	58.5	8,100	15,200	1.88
PF-Py*	56.4	8,900	18,300	2.06
PPE-Py	39.3	63,600	173,800	2.73
PPE-Py*	38.3	86,400	197,000	2.28
^{F}PPE-Py	59.9	–[c]	–[c]	–[c]
^{F}PPE-Py*	59.2	–[c]	–[c]	–[c]

[a] Fluorine content of the repeating unit. [b] Calculated by GPC using THF (1 mL·min^{-1}) as the mobile phase relative to PS standards. [c] Not soluble in the GPC mobile phase (THF).

RESULTS AND DISCUSSION

AFPs were synthesized by palladium-catalyzed cross-coupling polycondensation. **PF-Py** and **PF-Py*** were prepared via Suzuki polymerization between dibromide **1,** diboronate **2**, and the pyridine-containing dibromide (**Py** or **Py***) (**Scheme 1**). Although all the monomers were soluble in toluene, the Suzuki polymerization was performed in benzotrifluoride to solubilize the generated polymer that has fluorous characteristics.[38] In contrast, PPE polymers were synthesized by Sonogashira polymerization between diethylnyl [2.2.2] bridged bicyclic monomers **4** or **5**, diiodide **3**, and pyridine-containing diiodide

(**Py** or **Py***) in benzotrifluoride/diisopropylamine (3:2) (**Scheme 2**). All the polymers were purified by precipitation in methanol, followed by repeatedly washings with hot methanol, acetone and acetonitrile. The relative molecular weights and polydispersity indices were estimated by gel permeation chromatography (GPC) in THF solution using polystyrene standards (**Table 1**). However, **^{F}PPE** polymers were only soluble in fluorinated solvents, such as benzotrifluoride and hydrofluoroethers (e.g., HFE-7500 or HFE-7200), thereby preventing molecular weight determination by GPC. To evaluate the molecular weight, we made use of dynamic light scattering (DLS) in benzotrifluoride solution to calculate their radius of gyration. DLS analysis suggests an average radius of 20.8 nm for **^{F}PPE-Py** and 21.6 nm for **^{F}PPE-Py***, which are slightly larger than the persistence length of high molecular weight PPEs.[39-40]

The AFP UV-Vis absorption and fluorescence spectra were collected in dilute solutions of benzotrifluoride and in spin-casted films (**Figure 2**). Relevant photophysical data are collected in **Table 2**. The fact that the absorption and fluorescence profiles vary little between solution and thin films, suggests weak interpolymer interactions and confirms that the [2.2.2] bridged bicylic structures prevent polymer aggregation.[33-34] There is a general trend in emission bands to shift to longer wavelengths, as a result of enhanced energy migration to regions having more extended conjugation in solid structures. The influence of the thiophene-containing selector (**Py***) on the optical properties is significant, and all **Py***-polymers showed red-shifted absorption and emission maxima with respect to **Py** polymers without thiophene units. This suggests that the thiophene-bridge selectors should provide the ability to efficiently modulate the spectra with protonation.

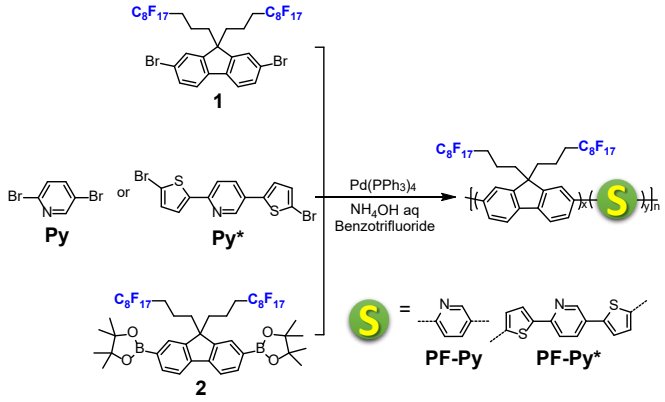

Scheme 1. Synthetic route to highly fluorous polyfluorenes (x= 0.80, y= 0.20).

The absence of aggregation endowed by the 2.2.2-bicyclic scaffolds in the polymer backbones prevents self-quenching to maintain high emission quantum yields, and makes for high reproducibility of spin-casted films. In the case of the **PF**s, some minor aggregation was observed, but overall the perfluoroalkane chains that extend perpendicular to the fluorene repeating units prevent close stacking of the conjugated backbones.[41] Moreover, **PF-Py*** showed two fluorescence peaks in solution, suggesting the presence of two different emissive species that probably correspond to **PF-Py*** and some minor polyfluorene oligomers without **Py*** receptors. The presence of oligomeric polyfluorene could not be detected by ^{1}H NMR nor GPC (**Figure S1**), but it was clearly observed in solution fluorescence measurements. In the solid state, the energy transfer is much more intense and the emission of the longer wavelength material dominates.

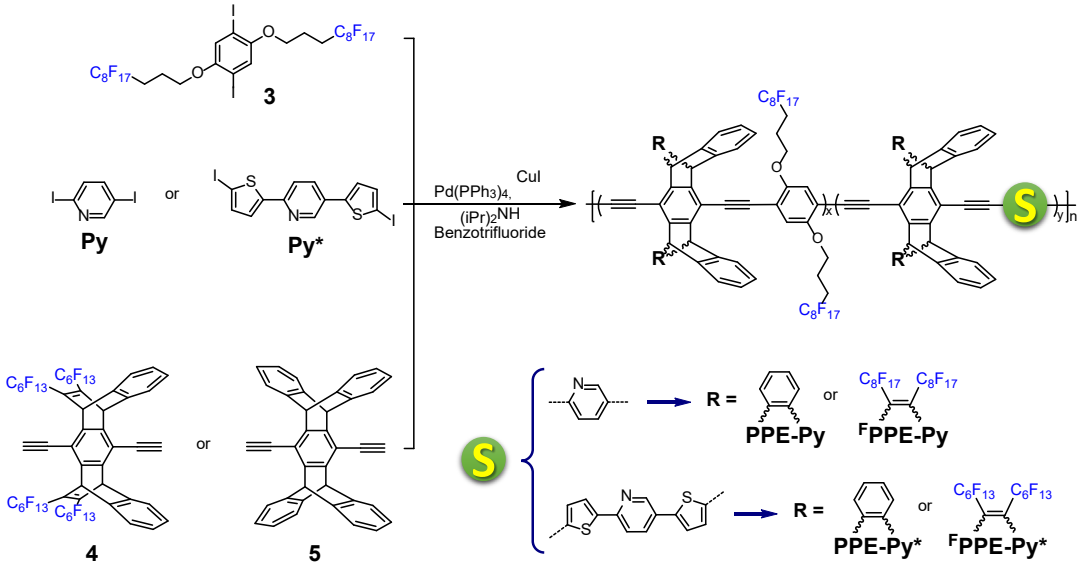

Scheme 2. Synthetic route to fluorous poly(*p*-phenylene ethynylenes) (x= 0.80, y= 0.20).

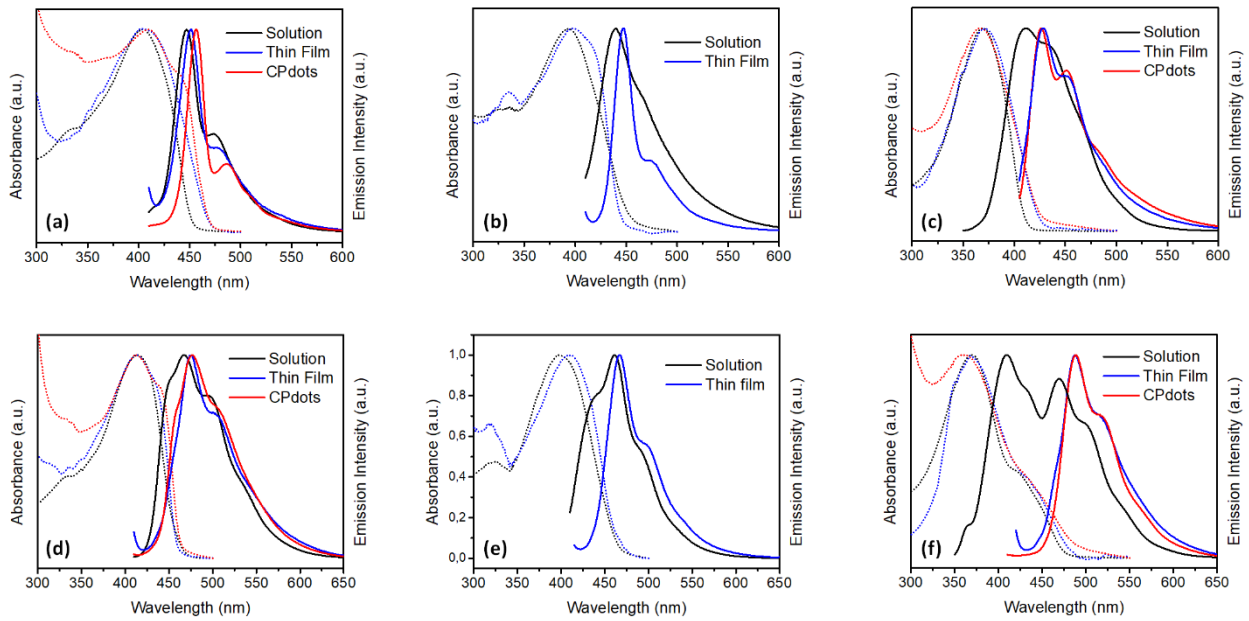

Figure 2. Absorption (dotted lines) and fluorescence (solid lines) spectra in benzotrifluoride solutions, spin-cast films, and CPdots: **(a) PPE-Py**, **(b) ^{F}PPE-Py**, **(c) PF-Py**, **(d) PPE-Py***, **(e) ^{F}PPE-Py***, and **(f) PF-Py***.

Table 2. Photophysical data.

	Media	λ_{abs} (nm)	λ_{em} (nm)
PF-Py	Benzotrifluoride	370	411
	Thin film	371	428
	CPdots	368	427
PF-Py*	Benzotrifluoride	369	410, 470
	Thin film	369	487
	CPdots	362	488
PPE-Py	Benzotrifluoride	404	447
	Thin film	406	451
	CPdots	407	456
PPE-Py*	Benzotrifluoride	413	467
	Thin film	413	475
	CPdots	413	476
^{F}PPE-Py	Benzotrifluoride	393	440
	Thin film	397	447
^{F}PPE-Py*	Benzotrifluoride	398	461
	Thin film	409	467

The fluorescence response of polymer thin films (30 to 50 Å thick) to aqueous solutions of PFOA was studied by introducing the films into sealed vials (20 mL capacity) containing 2.5 mL of different concentrations of PFOA in milliQ water. The mechanism of fluorescence change is the protonation of a nitrogen atom of a Lewis base (pyridine) and proton-transfer reactions are considered to occur nearly instantaneously,[42] as a result the most relevant and time-limiting factor that contributes to the fluorescence response is the time needed for PFOA molecules to diffuse from water to the fluorophilic polymer films.[35-37]

To ensure adequate PFAS diffusion into the films, we have used an exposure time of 1 hour to perform all our sensing experiments. Exposure of **PPE-Py** films to PFOA results in a broadening and red-shifting of the emission peak (from 451 to 490 nm), and visually the films change from having a blue to a bluish-green fluorescence (**Figure 3A**). This red shift is the result of the PFOA-induced protonation of pyridine units, which produces enhanced electro-accepting character and lowers the energy of charge transfer states. As a result of the amplifying nature of exciton migration, only a small percentage of pyridine acceptors need to be protonated to produce a large response.[29, 43] Thus, the short-wavelength shoulder of the initial fluorescence band probably suggests some residual emission from non-protonated **PPE-Py**. The **PPE-Py*** polymer showed a similar PFOA response, but the thiophenes produce a stronger change in emission with PFOA-induced protonation of pyridine units (**Figure 3B**). In particular, **PPE-Py*** films exhibited a blue to green visual fluorescence color change, together with a larger red-shifting of the initial band from 475 to 535 nm. The larger shift was expected as the thiophene-pyridine constructions were expected to have strong charge transfer character. **Figure 4** shows the calibration curves for both polymers, which are linear between 1 and 10 ppb. The limits of detection (LOD) were calculated to be 2 ppb (**PPE-Py**) and 1 ppb (**PPE-Py***). Moreover, we confirmed that film recycling was possible and most of the initial fluorescence of **PPE-Py** and **PPE-Py*** films can be recovered by rinsing with an aqueous NaOH (1 M) solution for 10 min and air drying (**Figure S2**).

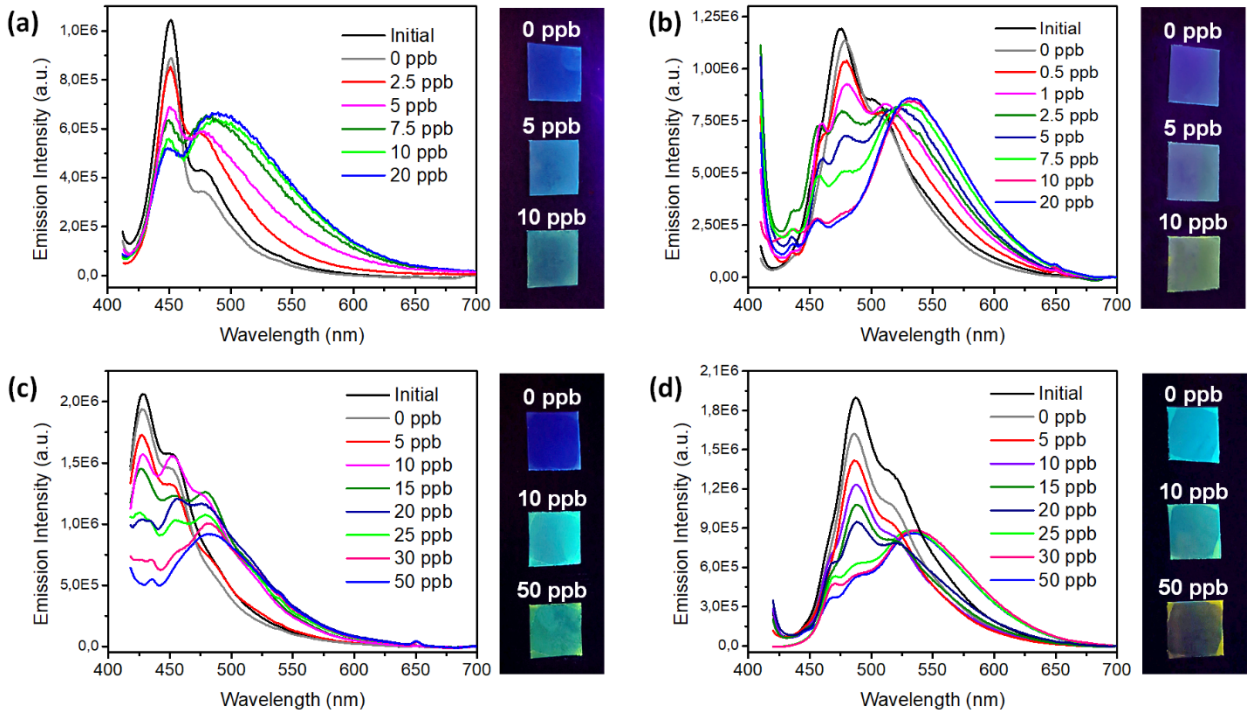

Figure 3. Fluorescence spectra of thin films upon exposure to aqueous solutions of PFOA, and the fluorescence photographs of the corresponding thin films: **(a) PPE-Py**, **(b) PPE-Py***, **(c) PF-Py**, and **(d) PF-Py***.

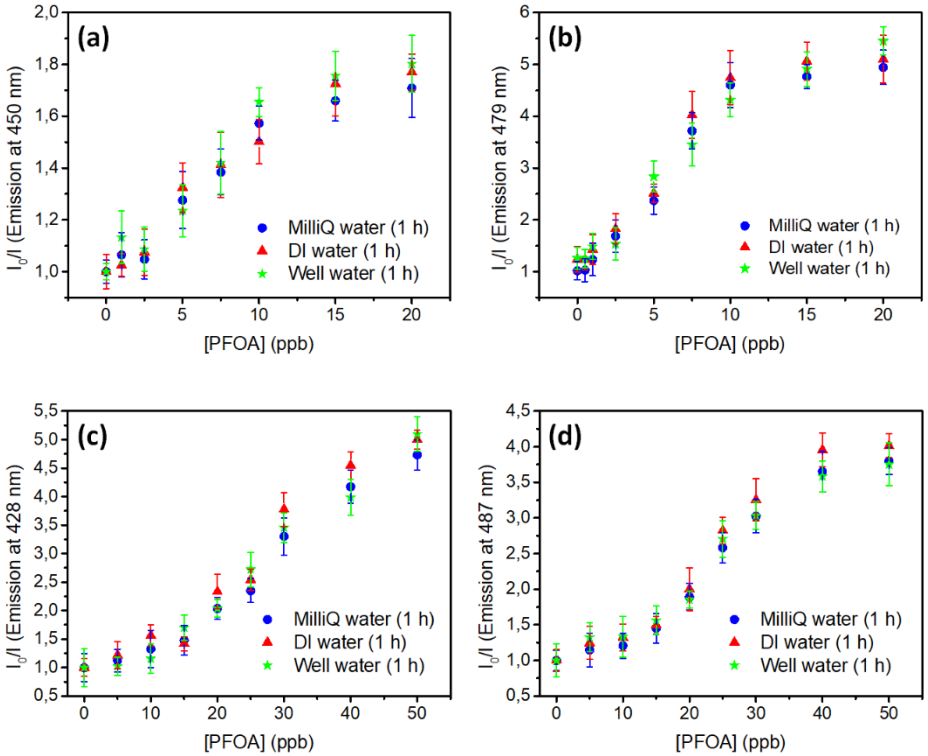

Figure 4. Changes in thin-film fluorescence intensity after exposure to PFOA in milliQ water, DI water, and well water (average values of three different films, error bars represent standard deviations): **(a) PPE-Py**, **(b) PPE-Py***, **(c) PF-Py**, **(d) PF-Py***.

^{F}PPE polymers are highly fluorinated AFPs with fluorine content of 60 wt. % (see **Table 1**). We initially hypothesized that **^{F}PPE** will exhibit higher sensibility as a result of the higher partitioning of PFAS into a more fluorous polymer film, but we observed more than two orders of magnitude lower sensitivity with LOD ~100 ppb relative to other **PPE** analogues (**Figure S3**). This considerably lower PFOA response is consistent with

^{F}PPE's highly hydrophobic nature and the poor wettability of the polymer film likely reduces PFOA diffusion into the film.

Exposure to PFOA causes the emission bands of **PF-Py** and **PF-Py*** to be broader, less-intense, and red-shifted. Bands shifted from 428 to 482 nm for **PF-Py** and from 487 to 535 nm for **PF-Py*** (**Figure 3C** and **3D**). As revealed by the photographs of the thin films in **Figure 3**, polymer films also showed visual detectable fluorescence color changes in response to PFOA. The evolution of the fluorescence intensity at the initial peak maximum for **PF-Py** and **PF-Py*** upon exposure to different PFOA concentrations (calibration curves) revealed linear regions from 10 to 40 ppb with calculated LOD of 8 ppb for **PF-Py** and 6 ppb for **PF-Py*** (**Figure 4**).

It is worth noticing that **PF-Py**/**PF-Py*** and **PPE-Py**/**PPE-Py*** AFPs have LOD of the same order of magnitude. This fact suggests that the diffusion of the PFOA into the polymers may be a limiting factor. In **PPE-Py**/**PPE-Py***, the 3D [2.2.2] fused bicyclic pentiptycene structures create porosity at the molecular level that is expected to enhance PFAS diffusion into the films. Nonetheless, the lack of porosity in films of **PF-Py**/**PF-Py*** is compensated with a higher fluorine content that enhances partition and association of aqueous PFOA into the polymer. However, it is clear that porosity and fluorous content must be considered along with other properties, and as stated earlier, **^{F}PPE-Py** and **^{F}PPE-Py*** are less sensitive, which we suggest is a consequence of an extremely hydrophilic nature and ineffective diffusion of PFOA from the water into the polymer solid.

We wondered if our detection method of PFOA, has general utility for sensing of other acidic PFAS, such as PFOS or perfluorobutanoic acid (PFBA). **PPE-Py*** is the AFP with the lowest LOD and we studied its fluorescence response to PFOS and PFBA. As shown in **Figure 5**, a clear fluorescence change was observed after exposing **PPE-Py*** polymer films to PFOS in milliQ and well water. The calibration curve reveals a linear region from 10 to 40 and a calculated LOD of 5 ppb. The higher LOD for PFOS (i.e., 5 ppb for PFOS and 1 ppb for PFOA) may be a result of the higher affinity of the sulfate, relative to a carboxylate, to be hydrated. It is likely that PFOS behaves as a surfactant at fluorous/water interface.[18] PFOS organized at the interfaces will not protonate the pyridines and lead to a reduced LOD. In the case of PFBA, exposure of **PPE-Py*** polymer films to different concentrations of PFBA resulted in a broadening and red-shifting of the emission bands, with similar detection limits to those obtained with PFOA (**Figure S4**). These results also indicate that our AFP sensors can selectively detect all different acidic PFAS, but they are not capable of differentiating between short- and long-chain PFAS.

Interestingly, **PPE-Py**/**PPE-Py*** and **PF-Py**/**PF-Py*** films did not exhibit fluorescence response when exposed to aqueous solutions of simple octanoic or butanoic acids, thereby demonstrating that fluorinated segments within the AFPs bind selectively PFAS (**Figure S5**). Our AFP-based sensor scheme relies on a relatively non-specific proton-transfer reaction and might be inherently susceptible to interferences from acidic and/or ionic species commonly found in groundwater. As a result, we decided to evaluate the potential interfering issues that may arise with complex aqueous matrices, such as groundwater. In particular, we selected well water collected from a well in Central Vermont as a realistic matrix to demonstrate the robustness of our AFP-based sensor. **Figure 4** shows the PFOA calibrations curves when the polymer films were immersed in milliQ water, DI water, and well water. We only observed minor deviations in the fluorescence responses to PFOA, and also the same detection limits within the margin of error.

To gain insight into the sensing mechanism, we studied direct interactions between PPE polymer backbone and PFAS. Therefore, we synthesized a PPE analogue without pyridine moieties (**PPE**) and studied its response to different concentrations of PFOA. Nonetheless, no variation of the emission was observed upon exposure of **PPE** films to PFOA (**Figure S6**), indicating that the unique PFAS response of our pyridine-containing AFPs is a consequence of pyridine protonation and not simply to direct interactions of PFAS with the polymer backbones. This fact was also confirmed by control experiments with non-acidic PFAS, such as methoxyperfluorobutane and 1H,2H,2H-perfluorooctanal hydrate that also partition into fluorous AFPs but are not capable of protonating pyridine moieties. In such control experiments under the same conditions, the emission of **PPE-Py*** films did not show any change upon exposure to methoxyperfluorobutane and 1H,2H,2H-perfluorooctanal hydrate (**Figure S7**), confirming that our fluorous AFP sensors are selective to acidic PFAS molecules.

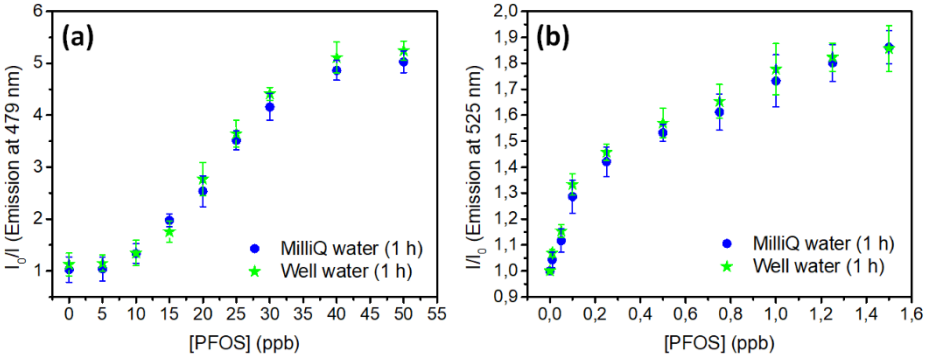

Figure 5. Changes in fluorescence intensity after exposure to PFOS in milliQ water, and well water (average values of three different measurements, error bars represent standard deviations): **(a)** thin-films of **PPE-Py**, and **(b) CPdots** of **PPE-Py***.

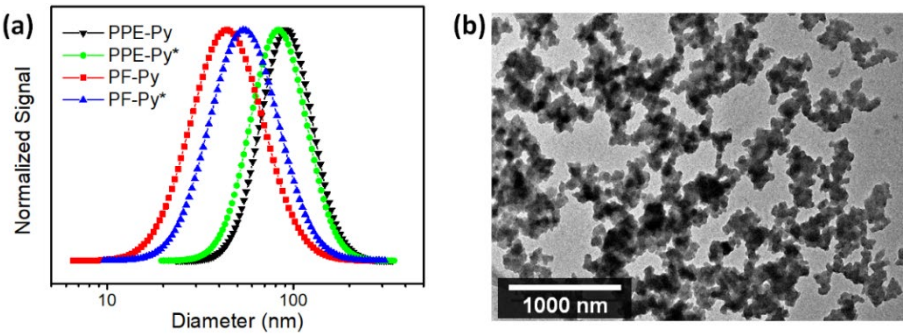

Figure 6. (a) DLS measurements of water dispersions of CPdots, **(b)** TEM image of **PPE-Py*** CPdots.

It is likely that the AFP sensing response is related to the diffusion of PFOA from water into the polymer film, which is dependent on the polymer/water interfacial area. Spin-cast AFP films have a limited surface area and to increase the polymer/water interface we prepared conjugated polymer nanoparticle (CPdot) dispersions in water. CPdots have found applications in imaging and chemical sensing,[44-49] and can be prepared by a reprecipitation method. Briefly, a dilute solution of the AFP in THF (0.01 mg·mL^{-1}, 2mL) was quickly added to water (8 mL) under sonication. THF was then evaporated under vacuum to yield optically clear aqueous dispersions of CPdots that display the same color as the starting THF solution. **^{F}PPE-Py** and **^{F}PPE-Py*** are not soluble in non-fluorinated solvents, complicating the formation of CPdots. As a result, CPdot studies focused on CPdots of **PPE-Py**, **PPE-Py***, **PF-Py**, and **PF-Py***. The resulting CPdots dispersions were stable over 1 month with no evidence of aggregation nor precipitation. The morphology of the CPdots and their size was evaluated by transmission electron microscopy (TEM) and DLS (**Figure 6**). TEM images showed the presence of spherical nanoparticles, which appeared to aggregate into interconnected networks. This aggregation has been previously observed for CPdots,[48] and just occurs during water evaporation in the sample preparation process due to the high hydrophobicity of our fluorinated polymers. In contrast, no aggregation of CPdots was detected in DLS experiments (PDI < 0.20), which gave monomodal size distributions with mean hydrodynamic diameters of 92 nm (**PPE-Py**), 83 nm (**PPE-Py***), 54 nm (**PF-Py**), and 44 nm (**PF-Py***).

The UV-Vis absorption spectra of the aqueous dispersions of the CPdots are broadened compared to those of the conjugated polymers in benzotrifluoride solution (**Figure 2**). Nonetheless, the absorption spectra of the **PF-Py**/**PF-Py*** CPdots have a slight blue-shifting from the solution state that is consistent with an overall reduction of the conjugated length of the AFP chain.[49] In contrast, the absorption spectra of **PPE-Py**/**PPE-Py*** CPdots did not show blue-shifting because the rigid iptycene repeating units may preclude the twisting of the polymer backbone and the reduction of its conjugation length. CPdots also exhibited red-shifted fluorescence spectra as compared to those of in solution, which is very similar to the spectra acquired in thin film form.

The fluorescence spectra of the CPdots were recorded after 1 hour incubation with different concentrations of PFOA in milliQ water (**Figure 7**). In accord with our thin film sensing experiments, PFOA exposure resulted in a broadening and red-shifting of the emission peaks. Moreover, those changes in the fluorescence spectra were accompanied by a visual change in the fluorescence color of the CPdot aqueous dispersions. These results confirmed that PFOA is able to diffuse into the CPdots and protonate the pyridine-based selectors, triggering changes in the fluorescent properties. **Figure 8** shows the calibration curves for the CPdots that reveal linear regions from ca. 0.05 to 1.5 ppb. We calculate a LOD of 0.2 ppb for **PPE-Py**, 0.08 ppb for **PPE-Py***, 0.8 ppb for **PF-Py**, and 0.7 ppb for **PF-Py***. These values are approximately one order of magnitude lower than those of found in thin film experiments, attesting to the impact of higher surface area.

We also determined that the CPdots performance is the same in milliQ water and well water (**Figure 8**). CPdots-based AFP sensors are also able to detect PFOS in addition to PFOA. CPdots of **PPE-Py*** showed a fluorescent response upon exposure to different concentrations of PFOS (**Figure 5**). The calibration curve for this data is linear from 0.1 to 1.5 ppb and gives a calculated LOD of 0.35 ppb. As explained, the higher LOD for PFOS is likely related to its different interfacial activity in comparison to PFOA.

In summary, our best performing polymer (i.e., **PPE-Py***) can selectively detect PFOA/PFOS concentrations of 1.0/5.0 ppb (2.4/9.9 nM) in thin film, and 0.08/0.35 ppb (0.2/0.7 nM) in CPdots forms. This PFAS sensitivity is superior to those of previously reported fluorescent sensors to our knowledge. For instance, the three most sensitive PFAS fluorescent sensors described so far consist of: (1) aggregation-induced emission chromophores deposited onto glass chips that can detect PFOA and PFOS concentrations of around 40 ppb (100 nM),[22] (2) an indicator displacement assay that uses guanidinocalix[5]arene and fluorescein and has LODs of 10.9 ppb (26.4 nM) for PFOA and 11.3 ppb (21.4 nM) for PFOS,[23] and (3) a fluorescent sensor array based on a library of macrocyclic species templated with a fluorophore that can detect PFAS at around 2.5 ppb (5 nM).[25] Nonetheless, although our AFPs-based sensors selectively detect acidic over non-acidic PFAS with the highest sensitivity reported for fluorescent sensors, they do not allow the differentiation between short- and long-chain PFAS, or distinguishing between different acidic functional groups. Our AFPs represent a proof-of-concept sensing assay that requires further optimization since its sensitivity is still insufficient to meet the recently announced US EPA legally enforceable levels in drinking water (4 ppt for PFOA and PFOS, individually), but it can be employed in heavily contaminated areas (e.g., around military facilities, airports, industrial areas…), or after preconcentrating the water sample with solid-phase extraction.

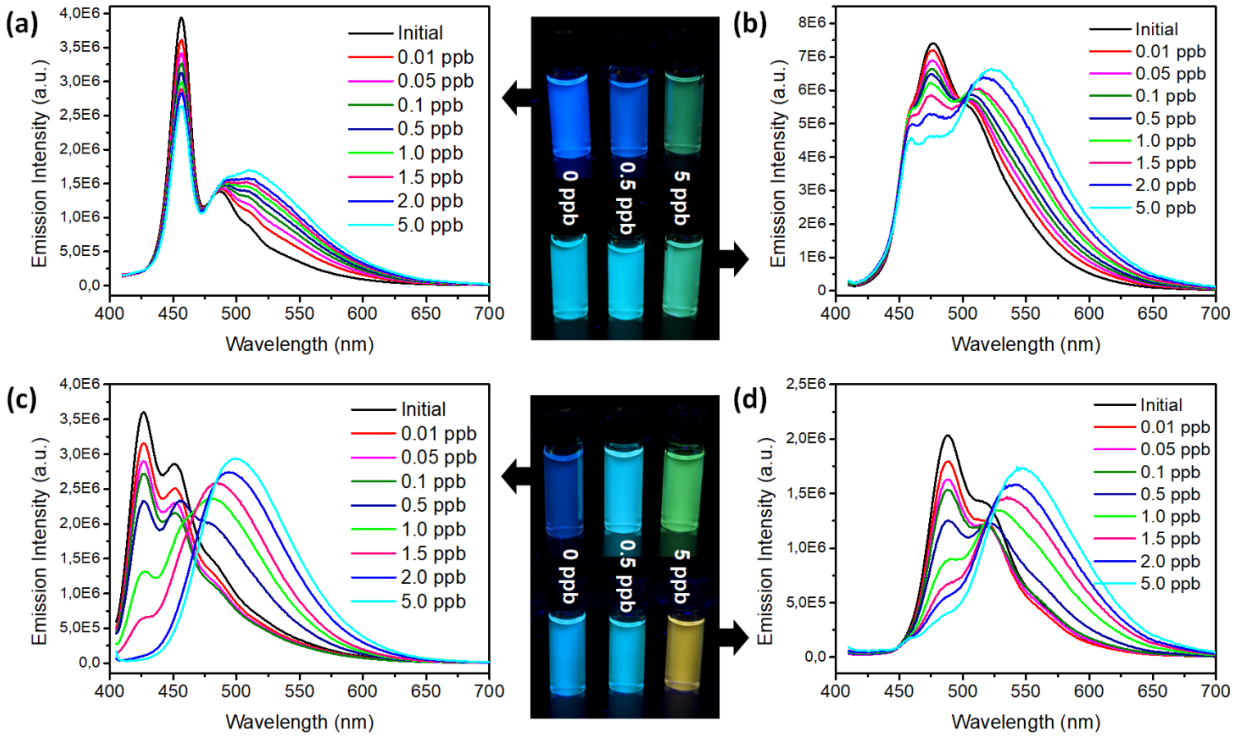

Figure 7. Fluorescence spectra of CPdots upon exposure to aqueous solutions of PFOA, and the fluorescence photographs of the corresponding CPdots dispersions: **(a) PPE-Py**, **(b) PPE-Py***, **(c) PF-Py**, **(d) PF-Py***.

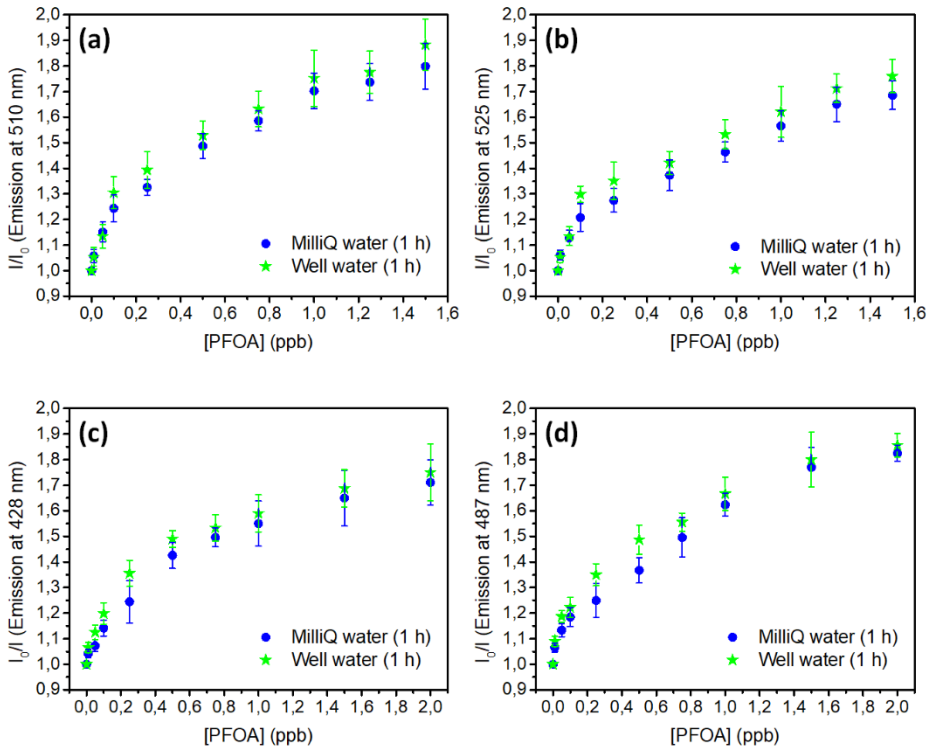

Figure 8. Changes in CPdots fluorescence intensity after exposure to PFOA in milliQ water and well water (average values of three different CPdots dispersions, error bars represent standard deviations): **(a) PPE-Py**, **(b) PPE-Py***, **(c) PF-Py**, **(d) PF-Py***.

CONCLUSIONS

In conclusion, we have developed amplifying fluorescent polymers (AFPs) that can selectively detect aqueous PFOA and PFOS in the ng·L^{-1} range. The AFPs are highly fluorinated and have poly(*p*-phenylene ethynylene) and polyfluorene backbones. Pyridine-based selectors were integrated into the AFPs that react with PFAS acids via a proton-transfer reaction. PFAS-

induced protonation of the pyridines creates lower-energy pyridinium traps for the excitons and emission from these sites results in a red shift of the spectra. These AFPs were initially evaluated as spin-coated films and can detect PFAS at concentrations of ~1 ppb. Higher surface area nanoparticles can detect aqueous PFAS concentrations of ~100 ppt. It is also noteworthy that both polymer films and nanoparticles are not affected by the type of water, and similar responses to PFAS were found in milliQ water, DI water, and well water. Although further optimization is needed to meet the current US EPA limits, the low detection limits make this sensor scheme potentially suitable for on-site PFAS detection in heavily contaminated areas. Further investigations of this approach and its utility to discriminate between short- and long-chain PFAS and to detect PFAS with different functional groups are currently ongoing in our laboratory.

ASSOCIATED CONTENT

Supporting Information. Materials and Characterization Techniques, Experimental Procedures, Synthesis and Characterization, Supplementary Figures. This material is available free of charge via the Internet at http://pubs.acs.org

AUTHOR INFORMATION

Corresponding Author

* tswager@mit.edu (T. M. S)

Present Address

‡ Instituto de Nanociencia y Materiales de Aragón (INMA), CSIC-University of Zaragoza-CSIC, 50009 Zaragoza, Spain.

Notes

The authors declare the following competing financial interest: A patent has been filed on this invention.

ACKNOWLEDGMENT

We are grateful for support from support from Xylem Corporation and the MIT Jameel Water and Food Security Center. J.C-E. acknowledges the financial support received from the Fulbright Program and the Xunta de Galicia (ED481B-2022-084). We also thank our colleagues Jessica C. Beard for helpful discussions, and Weize Yuan for TEM studies.

REFERENCES

1. Kannan, K., Perfluoroalkyl and polyfluoroalkyl substances: current and future perspectives. *Environ. Chem.* **2011,** *8* (4), 333-338.
2. Buck, R. C.; Franklin, J.; Berger, U.; Conder, J. M.; Cousins, I. T.; de Voogt, P.; Jensen, A. A.; Kannan, K.; Mabury, S. A.; van Leeuwen, S. P., Perfluoroalkyl and polyfluoroalkyl substances in the environment: Terminology, classification, and origins. *Integr. Environ. Assess. Manag.* **2011,** *7* (4), 513-541.
3. O'Hagan, D., Understanding organofluorine chemistry. An introduction to the C–F bond. *Chem. Soc. Rev.* **2008,** *37* (2), 308-319.
4. Bell, E. M.; De Guise, S.; McCutcheon, J. R.; Lei, Y.; Levin, M.; Li, B.; Rusling, J. F.; Lawrence, D. A.; Cavallari, J. M.; O'Connell, C.; Javidi, B.; Wang, X.; Ryu, H., Exposure, health effects, sensing, and remediation of the emerging PFAS contaminants – Scientific challenges and potential research directions. *Sci. Total Environ.* **2021,** *780*, 146399.
5. Graber, J. M.; Alexander, C.; Laumbach, R. J.; Black, K.; Strickland, P. O.; Georgopoulos, P. G.; Marshall, E. G.; Shendell, D. G.; Alderson, D.; Mi, Z.; Mascari, M.; Weisel, C. P., Per and polyfluoroalkyl substances (PFAS) blood levels after contamination of a community water supply and comparison with 2013–2014 NHANES. *J. Expo. Sci. Environ. Epidemiol.* **2019,** *29* (2), 172-182.
6. Sunderland, E. M.; Hu, X. C.; Dassuncao, C.; Tokranov, A. K.; Wagner, C. C.; Allen, J. G., A review of the pathways of human exposure to poly- and perfluoroalkyl substances (PFASs) and present understanding of health effects. *J. Expo. Sci. Environ. Epidemiol.* **2019,** *29* (2), 131-147.
7. Barry, V.; Winquist, A.; Steenland, K., Perfluorooctanoic Acid (PFOA) Exposures and Incident Cancers among Adults Living Near a Chemical Plant. *Environ. Health Perspect.* **2013,** *121* (11-12), 1313-1318.
8. Suja, F.; Pramanik, B. K.; Zain, S. M., Contamination, bioaccumulation and toxic effects of perfluorinated chemicals (PFCs) in the water environment: a review paper. *Water Science and Technology* **2009,** *60* (6), 1533-1544.
9. Rodriguez, K. L.; Hwang, J.-H.; Esfahani, A. R.; Sadmani, A. H. M. A.; Lee, W. H., Recent Developments of PFAS-Detecting Sensors and Future Direction: A Review. *Micromachines* **2020,** *11* (7), 667.
10. Fact Sheet on PFOA and PFOS Drinking Water Health Advisories. EPA 800-F-16-003; United States Environmental Protection Agency: Washington, D.C., 2016.
11. Technical Fact Sheet: Drinking Water Health Advisories for Four PFAS (PFOA, PFOS, GenX chemicals, and PFBS). EPA 822-F-22-002; United States Environmental Protection Agency: Washington, D.C., 2022.
12. Fact Sheet: EPA's Proposal to Limit PFAS in Drinking Water; United States Environmental Protection Agency: Washington, D.C., 2023.
13. Method 533: Determination of Per- and Polyfluoroalkyl Substances in Drinking Water by Isotope Dilution Anion Exchange Solid Phase Extraction and Liquid Chromatography/Tandem Mass Spectrometry. United States Environmental Protection Agency, Washington, D.C., 2019.
14. Method 537.1 Determination of Selected Per- and Polyflourinated Alkyl Substances in Drinking Water by Solid Phase Extraction and Liquid Chromatography/Tandem Mass Spectrometry (LC/MS/MS). United States Environmental Protection Agency, Washington, D.C., 2020.
15. Wang, Y.; Darling, S. B.; Chen, J., Selectivity of Per- and Polyfluoroalkyl Substance Sensors and Sorbents in Water. *ACS Appl. Mater. Interfaces* **2021,** *13* (51), 60789-60814.
16. Garg, S.; Kumar, P.; Greene, G. W.; Mishra, V.; Avisar, D.; Sharma, R. S.; Dumée, L. F., Nano-enabled sensing of per-/poly-fluoroalkyl substances (PFAS) from aqueous systems – A review. *J. Environ. Manage.* **2022,** *308*, 114655.
17. Al Amin, M.; Sobhani, Z.; Liu, Y.; Dharmaraja, R.; Chadalavada, S.; Naidu, R.; Chalker, J. M.; Fang, C., Recent advances in the analysis of per- and polyfluoroalkyl substances (PFAS)—A review. *Environ. Technol. Innov.* **2020,** *19*, 100879.
18. Trinh, V.; Malloy, C. S.; Durkin, T. J.; Gadh, A.; Savagatrup, S., Detection of PFAS and Fluorinated Surfactants Using Differential Behaviors at Interfaces of Complex Droplets. *ACS Sensors* **2022,** *7* (5), 1514-1523.
19. Sahu, S. P.; Kole, S.; Arges, C. G.; Gartia, M. R., Rapid and Direct Perfluorooctanoic Acid Sensing with Selective Ionomer Coatings on Screen-Printed Electrodes under Environmentally Relevant Concentrations. *ACS Omega* **2022,** *7* (6), 5001-5007.
20. Faiz, F.; Baxter, G.; Collins, S.; Sidiroglou, F.; Cran, M., Polyvinylidene fluoride coated optical fibre for detecting perfluorinated chemicals. *Sens. Actuators B Chem.* **2020,** *312*, 128006.
21. Clark, R. B.; Dick, J. E., Electrochemical Sensing of Perfluorooctanesulfonate (PFOS) Using Ambient Oxygen in River Water. *ACS Sensors* **2020,** *5* (11), 3591-3598.
22. Fang, C.; Wu, J.; Sobhani, Z.; Amin, M. A.; Tang, Y., Aggregated-fluorescent detection of PFAS with a simple chip. *Anal. Methods* **2019,** *11* (2), 163-170.
23. Zheng, Z.; Yu, H.; Geng, W.-C.; Hu, X.-Y.; Wang, Y.-Y.; Li, Z.; Wang, Y.; Guo, D.-S., Guanidinocalix[5]arene for sensitive fluorescence detection and magnetic removal of perfluorinated pollutants. *Nat. Commun.* **2019,** *10* (1), 5762.
24. Ranaweera, R.; Ghafari, C.; Luo, L., Bubble-Nucleation-Based Method for the Selective and Sensitive Electrochemical Detection of Surfactants. *Anal. Chem.* **2019,** *91* (12), 7744-7748.

25. Harrison, E. E.; Waters, M. L., Detection and differentiation of per- and polyfluoroalkyl substances (PFAS) in water using a fluorescent imprint-and-report sensor array. *Chem. Sci.* **2023,** *14* (4), 928-936.
26. Rochat, S.; Swager, T. M., Conjugated Amplifying Polymers for Optical Sensing Applications. *ACS Appl. Mater. Interfaces* **2013,** *5* (11), 4488-4502.
27. Thomas, S. W.; Joly, G. D.; Swager, T. M., Chemical Sensors Based on Amplifying Fluorescent Conjugated Polymers. *Chem. Rev.* **2007,** *107* (4), 1339-1386.
28. Zhou, Q.; Swager, T. M., Method for enhancing the sensitivity of fluorescent chemosensors: energy migration in conjugated polymers. *J. Am. Chem. Soc.* **1995,** *117* (26), 7017-7018.
29. Zhou, Q.; Swager, T. M., Fluorescent Chemosensors Based on Energy Migration in Conjugated Polymers: The Molecular Wire Approach to Increased Sensitivity. *J. Am. Chem. Soc.* **1995,** *117* (50), 12593-12602.
30. Swager, T. M., Sensor Technologies Empowered by Materials and Molecular Innovations. *Angew. Chem. Int. Ed.* **2018,** *57*, 4248-4257.
31. Cumming, C. J.; Aker, C.; Fisher, M.; Fok, M.; Grone, M. J. l.; Reust, D.; Rockley, M. G.; Swager, T. M.; Towers, E.; Williams, V., Using novel fluorescent polymers as sensory materials for above-ground sensing of chemical signature compounds emanating from buried landmines. *IEEE Transactions on Geoscience and Remote Sensing* **2001,** *39* (6), 1119-1128.
32. Cox, J. R.; Müller, P.; Swager, T. M., Interrupted Energy Transfer: Highly Selective Detection of Cyclic Ketones in the Vapor Phase. *J. Am. Chem. Soc.* **2011,** *133* (33), 12910-12913.
33. Yang, J.-S.; Swager, T. M., Porous Shape Persistent Fluorescent Polymer Films: An Approach to TNT Sensory Materials. *J. Am. Chem. Soc.* **1998,** *120* (21), 5321-5322.
34. Yang, J.-S.; Swager, T. M., Fluorescent Porous Polymer Films as TNT Chemosensors: Electronic and Structural Effects. *J. Am. Chem. Soc.* **1998,** *120* (46), 11864-11873.
35. Wang, R.; Lin, Z.-W.; Klemes, M. J.; Ateia, M.; Trang, B.; Wang, J.; Ching, C.; Helbling, D. E.; Dichtel, W. R., A Tunable Porous β-Cyclodextrin Polymer Platform to Understand and Improve Anionic PFAS Removal. *ACS Cent. Sci.* **2022,** *8* (5), 663-669.
36. Wu, C.; Klemes, M. J.; Trang, B.; Dichtel, W. R.; Helbling, D. E., Exploring the factors that influence the adsorption of anionic PFAS on conventional and emerging adsorbents in aquatic matrices. *Water Res.* **2020,** *182*, 115950.
37. Xiao, L.; Ling, Y.; Alsbaiee, A.; Li, C.; Helbling, D. E.; Dichtel, W. R., β-Cyclodextrin Polymer Network Sequesters Perfluorooctanoic Acid at Environmentally Relevant Concentrations. *J. Am. Chem. Soc.* **2017,** *139* (23), 7689-7692.
38. Lee, J.-K.; Fong, H. H.; Zakhidov, A. A.; McCluskey, G. E.; Taylor, P. G.; Santiago-Berrios, M. e.; Abruña, H. D.; Holmes, A. B.; Malliaras, G. G.; Ober, C. K., Semiperfluoroalkyl Polyfluorenes for Orthogonal Processing in Fluorous Solvents. *Macromolecules* **2010,** *43* (3), 1195-1198.
39. Lim, J.; Swager, T. M., Fluorous Biphase Synthesis of a Poly(p-phenyleneethynylene) and its Fluorescent Aqueous Fluorous-Phase Emulsion. *Angew. Chem. Int. Ed.* **2010,** *49* (41), 7486-7488.
40. Cotts, P. M.; Swager, T. M.; Zhou, Q., Equilibrium Flexibility of a Rigid Linear Conjugated Polymer. *Macromolecules* **1996,** *29* (23), 7323-7328.
41. Bouffard, J.; Swager, T. M., Fluorescent Conjugated Polymers That Incorporate Substituted 2,1,3-Benzooxadiazole and 2,1,3-Benzothiadiazole Units. *Macromolecules* **2008,** *41* (15), 5559-5562.
42. Donten, M. L.; VandeVondele, J.; Hamm, P., Speed Limits for Acid–Base Chemistry in Aqueous Solutions. *CHIMIA* **2012,** *66* (4), 182.
43. Swager, T. M., The Molecular Wire Approach to Sensory Signal Amplification. *Acc. Chem. Res.* **1998,** *31* (5), 201-207.
44. Wu, C.; McNeill, J., Swelling-Controlled Polymer Phase and Fluorescence Properties of Polyfluorene Nanoparticles. *Langmuir* **2008,** *24* (11), 5855-5861.
45. Wu, C.; Szymanski, C.; Cain, Z.; McNeill, J., Conjugated Polymer Dots for Multiphoton Fluorescence Imaging. *J. Am. Chem. Soc.* **2007,** *129* (43), 12904-12905.
46. Wu, C.; Szymanski, C.; McNeill, J., Preparation and Encapsulation of Highly Fluorescent Conjugated Polymer Nanoparticles. *Langmuir* **2006,** *22* (7), 2956-2960.
47. Wu, C.; Peng, H.; Jiang, Y.; McNeill, J., Energy Transfer Mediated Fluorescence from Blended Conjugated Polymer Nanoparticles. *J. Phys. Chem. B* **2006,** *110* (29), 14148-14154.
48. Szymanski, C.; Wu, C.; Hooper, J.; Salazar, M. A.; Perdomo, A.; Dukes, A.; McNeill, J., Single Molecule Nanoparticles of the Conjugated Polymer MEH−PPV, Preparation and Characterization by Near-Field Scanning Optical Microscopy. *J. Phys. Chem. B* **2005,** *109* (18), 8543-8546.
49. Kurokawa, N.; Yoshikawa, H.; Hirota, N.; Hyodo, K.; Masuhara, H., Size-Dependent Spectroscopic Properties and Thermochromic Behavior in Poly(substituted thiophene) Nanoparticles. *ChemPhysChem* **2004,** *5* (10), 1609-1615.

Insert Table of Contents artwork here